Excited Singlet States of Covalently Bound, Cofacial Dimers and Trimers of Perylene-3,4:9,10-bis(dicarboximide)s

Jovan M. Giaimo, Jenny V. Lockard, Louise E. Sinks, Amy M. Scott, Thea M. Wilson, and Michael R. Wasielewski*

Department of Chemistry and Argonne-Northwestern Solar Energy Research (ANSER) Center, Northwestern University, Evanston, Illinois 60208-3113

Received: November 13, 2007; In Final Form: January 7, 2008

Perylene-3,4:9,10-bis(dicarboximide) (PDI) and its derivatives are robust organic dyes that strongly absorb visible light and display a strong tendency to self-assemble into ordered aggregates, having significant interest as photoactive materials in a wide variety of organic electronics. To better understand the nature of the electronics states produced by photoexcitation of such aggregates, the photophysics of a series of covalent, cofacially oriented, π-stacked dimers and trimers of PDI and 1,7-bis(3′,5′-di-*t*-butylphenoxy)perylene-3,4:9,10-bis(dicarboximide) (PPDI) were characterized using both time-resolved absorption and fluorescence spectroscopy. The covalent linkage between the chromophores was accomplished using 9,9-dimethylxanthene spacers. Placing *n*-octyl groups on the imide nitrogen atoms at the end of the PDI chromophores not attached to the xanthene spacer results in PDI dimers having near optimal π-stacking, leading to formation of a low-energy excimer-like state, while substituting the more sterically demanding 12-tricosanyl group on the imides causes deviations from the optimum that result in slower formation of an excimer-like excited state having somewhat higher energy. By comparison, PPDI dimers having terminal *n*-octyl imide groups have two isomers, whose photophysical properties depend on the ability of the phenoxy groups at the 1,7-positions to modify the π stacking of the PPDI molecules. In general, disruption of optimal π-stacking by steric interactions of the phenoxy side groups results in excimer-like states that are higher in energy. The corresponding lowest excited singlet states of the PDI and PPDI trimers are dimer-like in nature and suggest that structural distortions that accompany formation of the trimers are sufficient to confine the electronic interaction on two chromophores within these systems. This further suggests that it may be useful to build into oligomeric PDI and PPDI systems some degree of flexibility that allows the structural relaxations necessary to promote electronic interactions between multiple chromophores.

Introduction

Molecular materials offer many advantages for the development of novel electronic and photonic devices including ease of fabrication, mechanical flexibility, low processing temperatures, compatibility with plastic substrates, and/or high area coverage at low cost.[1−4] For example, the use of organic molecules, such as oligoacenes,[5−7] porphyrins,[8,9] and phthalocyanines,[10] in field effect transistors (OFETs), photovoltaics (OPVs), and light emitting diodes (OLEDs) is increasingly common. The performance of these materials as charge or energy transport materials depends not only on optimizing the electronic properties of the individual molecules, but depends as well on favorable intermolecular interactions, such as π-stacking and hydrogen bonding to assemble larger functional structures. Many novel approaches to self-assembly of individual building blocks into π-stacked functional structures mimic key strategies found in photosynthetic light harvesting proteins[11−13] and DNA.[14−16]

Perylene-3,4:9,10-bis(dicarboximide) (PDI) and its derivatives have attracted significant interest as active materials for light harvesting,[17−21] photovoltaics,[10,22−28] and studies of basic photoinduced charge and energy transfer processes.[29−34] PDI is both photochemically and thermally stable[35] and can be easily modified at its imide nitrogens, and its 1, 6, 7, and 12 positions. Modifications at these positions tune the electronic properties of PDI resulting in derivatives that absorb light from the near-ultraviolet to the near-infrared region of the spectrum. Moreover, the redox potentials of PDI can be tuned by appropriate substituents resulting in derivatives that are either good electron acceptors[36] or donors.[37] PDI also demonstrates the ability to self-assemble in solution via hydrophobic/hydrophilic interactions as well as by $\pi-\pi$ stacking.[38−43] Self-assembled, π-stacked PDI systems have been studied extensively; these systems include 1-D assemblies of PDI with a solubilizing group consisting of long alkyl chains at the imide position,[44] tethered, extended PDI systems,[41,42,45−52] tetra-substituted phenoxy PDI,[53−56] bis-1,7-(3′,5′-di-*t*-butylphenoxy)-PDI (PPDI),[38,57,58] and controlled assemblies of PPDI dimers.[59,60] We have recently investigated covalent PDI- and PPDI-based electron donor−acceptor systems that self-assemble to form larger structures for energy and electron transport.[38,60−63] Many of these systems take advantage of the tendency of these chromophores to form *H*-aggregates having roughly cofacial orientations. This promotes enhanced electronic communication between adjacent chromophores, enabling efficient energy and/or charge transport.

We present here the synthesis and photophysical properties of a series of PDI and PPDI covalently bound cofacial dimers and trimers, Figure 1. These molecules employ a xanthene

* Corresponding author. E-mail: m-wasielewski@northwestern.edu.

10.1021/jp710847q CCC: $40.75
Published on Web 02/26/2008

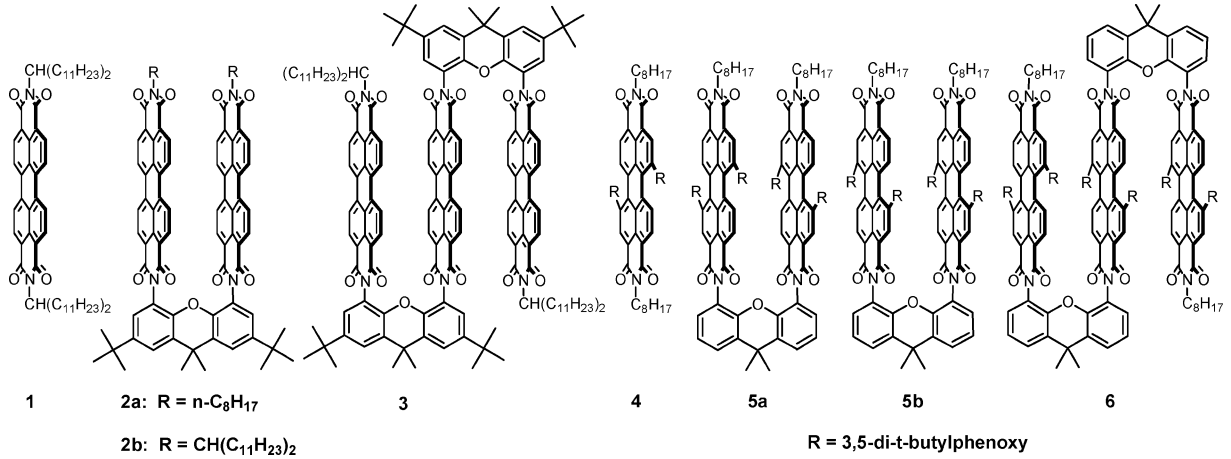

Figure 1. Structures of molecules used in this study.

bridge that strongly restricts the distances and orientations between the adjacent chromophores.[64] Two different types of PDI and PPDI chromophores are investigated: one in which the terminal imide is substituted with an *n*-octyl group and one in which the terminal imide is substituted with a more sterically demanding 12-tricosanyl group. The electronic absorption spectra of the cofacially stacked PDI and PPDI molecules exhibit an intensity redistribution of the Franck−Condon progression that effectively blue-shifts the peak maximum relative to that of the corresponding monomer species. The steady-state emission spectra of the cofacially stacked molecules are broad and red-shifted as compared to those of the corresponding monomer molecules. While similar spectral changes have been observed previously in PDI and PPDI systems,[35,41,42,45,46,65] the data presented in this Article probe how the photophysical properties of covalent, cofacial dimers and trimers depend on structural changes that occur as a result of changing substituents on the PDI.

Experimental Section

Toluene was purified by passing it through series of CuO and alumina columns. The synthesis of **1** was reported earlier,[66] while those of **2a**−**6** are detailed in the Supporting Information. Proton nuclear magnetic resonance spectra were recorded on Mercury 400 or Inova 500 NMR spectrometers using TMS as an internal standard. Mass spectrometry measurements were made on a PE Voyager DE-Pro MALDI-TOF mass spectrometer. High-resolution electrospray and fast atom bombardment mass spectra were obtained with the 70-SE-4F and Q-tof Ultima mass spectrometers at the University of Illinois at Urbana−Champaign.

Steady-state absorption was measured on a Shimadzu 1601 UV−vis spectrophotometer. Steady-state emission was measured on a PTI Quanta-Master 1 single photon counting spectrofluorimeter in a right angle configuration. A 10-mm fused silica cuvette was used for both absorption and emission experiments. The optical density at the absorption maximum (λ_{max}) for the fluorescence measurements was maintained at 0.1 ± 0.05 to avoid reabsorption artifacts. Oxazine 170 perchlorate in methanol ($\Phi_{fl} = 0.63$)[67] or Rhodamine 6G in absolute ethanol ($\Phi_{fl} = 0.95$)[68] were used as standards to determine relative fluorescence quantum yields. For the variable-temperature fluorescence measurements, the sample temperature was maintained to within ±0.1 K by a thermostated cell holder (Quantum Northwest Flash 100). The sample was allowed to equilibrate for 20 min at each temperature prior to the fluorescence measurement.

Femtosecond transient absorption measurements were made using a previously described regeneratively amplified titanium: sapphire laser system operating at a 2 kHz repetition rate outfitted with a CCD array detector (Ocean Optics PC2000) for simultaneous collection of spectral and kinetic data.[59,69] All samples were filtered through a 0.45 μm PTFE filter before measurement in a 2 mm quartz cuvette. The frequency-doubled output from the laser provides 414 nm, 120 fs pulses to pump an OPA, which generates tunable excitation pulses at 470−750 nm. Focusing a few microjoules of the 800 nm fundamental into a 3 mm sapphire disk generated a white light continuum probe pulse. All-reflective optics were used to focus the 800 nm pulse into the sapphire and recollimate the white light output, thus limiting the chirp on the white light pulse to <200 fs from 450 to 800 nm. Cuvettes with a 2 mm path length were used, and the samples were irradiated with 1.0 μJ/pulse focused to a 200 μm spot. The optical density at λ_{max} was typically 0.8 ($\sim 10^{-4}$ M). The total instrument response function (IRF) for the pump−probe experiments was 180 fs. Kinetics were determined at several wavelengths using a nonlinear least-squares fit to a general sum of exponentials using the Levenberg−Marquardt algorithm, while accounting for the presence of the finite instrument response.

Nanosecond transient absorption measurements were made using a Continuum Panther OPO pumped by the frequency-tripled output of a Continuum 8000 Nd:YAG laser. The probe light in the nanosecond experiment was generated using a xenon flashlamp (EG&G Electrooptics FX-200) and detected using a photomultiplier tube with high voltage applied to only four dynodes (Hamamatsu R928). The total IRF is 7 ns and is determined primarily by the laser pulse duration.

Fluorescence lifetime measurements were made using a Hamamatsu C4780 picosecond fluorescence lifetime measurement system, consisting of a C4334 Streakscope and a C4792-01 synchronous delay generator. The excitation light source was supplied by a home-built cavity-dumped Ti:sapphire laser[70] with a NEOS N13389 3-mm fused-silica acoustooptic modulator (AOM). The AOM was driven by an NEOS Technologies N64389-SYN 10 W driver to deliver 30 nJ, sub-50 fs pulses at an 820 kHz repetition rate. The laser pulses were frequency doubled to 400 nm by focusing the 800 nm fundamental into a 0.3 mm type I BBO crystal. The energy of the resulting blue pulses was attenuated to approximately 0.5 nJ/pulse for all fluorescence lifetime experiments. The total IRF of the streak camera system was 20 ps. The samples were prepared in glass cuvettes, and the optical density at the excitation wavelength

was typically 0.020−0.035. At λ_{max} of the samples, the optical density was typically 0.080−0.105. All fluorescence data were acquired in single-photon-counting mode using the Hamamatsu HPD-TA software. The data were fit using the Hamamatsu fitting module and deconvoluted using the laser pulse profile.

Results

Synthesis and Structure. Dimers **2a** and **2b** were synthesized by heating an imidazole solution of *N*-(*n*-octyl)- and *N*-(12-tricosanyl)perylene-3,4-dicarboxyanhydride-9,10-dicarboximide, respectively, with 4,5-diamino-2,3-di-*t*-butyl-9,9-dimethylxanthene to 160 °C. Similarly, an isomeric mixture of **5a** and **5b** was prepared by heating an imidazole solution of *N*-(*n*-octyl)-1,7-(3′,5′-di-*t*-butylphenoxy)perylene-3,4-dicarboxyanhydride-9,10-dicarboximide and the same 4,5-diamino-9,9-dimethylxanthene derivative to 160 °C. Isomeric dimers **5a** and **5b** were separated using flash chromatography on silica gel. The syntheses of trimers **3** and **6** followed similar schemes. Briefly, combining the *N*-alkyl perylene-imide-anhydride with an excess of the xanthenediamine yielded the singly substituted PDI-xantheneamine compound. Reaction of this PDI-xantheneamine with 0.5 equiv of the corresponding perylenedianhydride produced the trimer. In the case of **6**, separation of the three trimer isomers required HPLC (Supporting Information, Figure S1) and resulted in isolation of the dominant (85−92%) isomer (see below) shown in Figure 1.

9,9-Dimethylxanthene is C_2 symmetric with both methyls at the 9-position being equivalent. Thus, for the PDI series having no 1,7-substituents, **2a**, **2b**, and **3**, the ^{1}H NMR resonances of the methyl groups on the xanthene appear as singlets at 1.87 (6H), 1.85 (6H), and 1.82 (12H) ppm, respectively, which is consistent with an overall symmetric magnetic environment at that position in these molecules. On the other hand, in the cofacially stacked PPDI series, the two methyl groups on the xanthene spacer experience different magnetic environments depending on which isomer is present, and thus their ^{1}H NMR resonances serve to identify the isomers. In **5a**, both methyl groups on the xanthene appear as a single resonance at 1.76 (6H) ppm, indicating that both methyl groups are equivalent and that the phenoxy groups of the PPDIs must be arranged in a staggered conformation. In **5b**, the two methyl groups of the xanthene appear as a pair of singlets at 1.76 (3H) and 1.80 (3H) ppm, indicating that the asymmetric placement of the phenoxy groups relative to the two xanthene methyl groups leads to two different magnetic environments supporting the eclipsed conformation of the phenoxy groups. The xanthene methyl groups in **6** exhibit three singlets at 1.70 (6H) ppm, 1.80 (3H) ppm, and 1.85 (3H) ppm. The three different methyl resonances suggest that the phenoxy groups of the middle PPDI in **6** are in a staggered conformation relative to those of one of the outer PPDI molecules and in an eclipsed conformation relative to those in the other outer PPDI, Figures S2 and S3.

Steady-State Absorption and Emission Spectroscopy. The electronic absorption spectra of **1**, **2a**, **2b**, and **3** in chloroform are provided in Figure 2. Molecule **1** has an absorption maximum at 527 nm with the lower intensity vibronic peaks at 490 and 458 nm. The peak spacing of this vibronic progression is ∼1400 cm^{-1}. This vibrational mode frequency is associated with an out-of-phase C−C stretch of the perylene core.[71] Cofacial π-stacking of PDI in **2a** results in a new absorption maximum at 491 nm. The absorbance of **2b** exhibits spectral changes as compared to **1** that are similar to those observed in **2a**. The absorption maximum of **2b** is at 491 nm, which is also blue-shifted relative to that of the monomer. The addition of

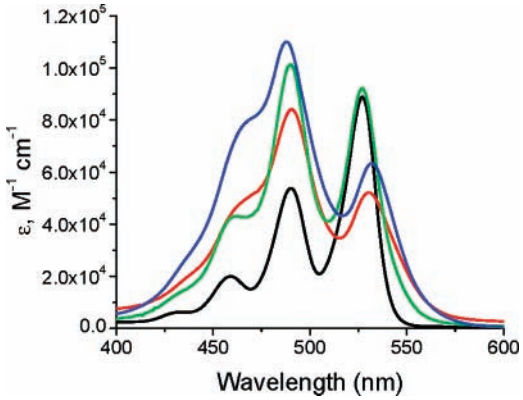

Figure 2. Ground-state absorption spectra of **1** (black), **2a** (red), **2b**, (green), and **3** (blue) in chloroform.

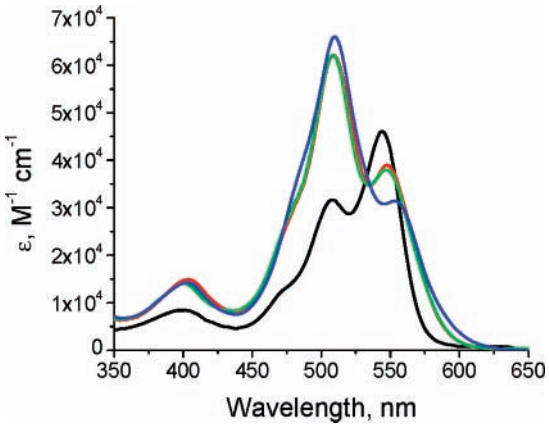

Figure 3. Ground-state absorption spectra of **4** (black), **5a** (red), **5b** (green), and **6** (blue) in toluene.

the third PDI chromophore in **3** slightly increases the observed splitting between the first two peaks of the absorption spectrum, Figure 2. The absorption maximum of **3** is at 488 nm, while the lowest energy peak is at 533 nm.

The absorption spectra of **4**, **5a**, **5b**, and **6** in toluene are provided in Figure 3. The absorption spectrum of **4** is characterized by a maximum at 545 nm with a smaller peak at 510 nm. **5a** and **5b** display nearly identical UV−vis spectra with maxima occurring at 508 nm and a smaller peak near the maximum of the monomer at 547 nm. The absorption maximum of **6** occurs at 508 nm with a smaller peak at 553 nm. The spectrum of **6** is slightly broader than those of **5a** and **5b**.

The normalized steady-state fluorescence spectra of **1**, **2a**, **2b**, and **3** in toluene are provided in Figure 4, and their fluorescence quantum yields are compiled in Table 1. Compound **1** has a sharp, well-resolved fluorescence spectrum with an emission maximum at 534 nm and vibronic bands at 576 and 624 nm, while emission from **2a** is broad and featureless with an emission maximum at 735 nm. The emission spectrum of the corresponding isomer **2b** is characterized by a maximum at 647 nm with shoulders at 611 and 561 nm. It is noteworthy that the fluorescence quantum yield of **2b** (0.19) is much larger than that of **2a** (0.02). The emission from **3** has an emission maximum at 647 nm and quantum yield that is similar to that of **2b**. The data in Figure 5 show that the fluorescence spectrum of dimer **2b** at −10 °C is dominated by a broad featureless band at 677 nm with minor shoulders at 560 and 610 nm, while at 60 °C the 677 nm band blue-shifts, and the 560 and 610 nm shoulders grow at the expense of the broad red-shifted band resolving into peaks at 555 and 598 nm.

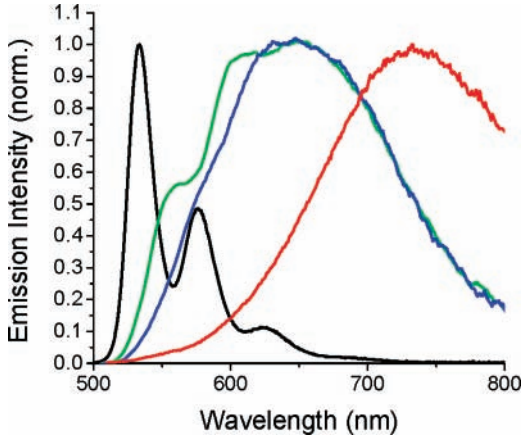

Figure 4. Fluorescence spectra of **1** (black), **2a** (red), **2b** (green), and **3** (blue) in toluene (excited at 490 nm). The emission intensities are normalized at their maxima.

TABLE 1: Photophysical Data in Toluene at 295 K[a]

compound	$\lambda_{abs\ max}$ (nm)	$\lambda_{ems\ max}$ (nm)	ϕ_{FL}	time-resolved fluorescence data: λ_{ems} (nm)	time-resolved fluorescence data: τ_{FL} (ns)
1	527	533	0.98	550	3.8 ± 0.1
2a	490	735	0.02	700	9.2 ± 0.1
2b	491	647	0.19	550	0.05 ± 0.01
				700	28.6 ± 0.1
3	488	647	0.13	550	0.05 ± 0.01
				700	22.5 ± 0.1
4	545	568	0.98	550	4.5 ± 0.1
5a	509	705	0.08	700	21.1 ± 0.1
5b	509	675	0.06	700	18.6 ± 0.1
6	510	679	0.26	700	36.5 ± 0.1

[a] Fluorescence spectra and lifetimes are determined using 400 excitation. Lifetimes are obtained by fitting of the observed kinetics to a convolution of the instrument response function and a sum of exponentials.

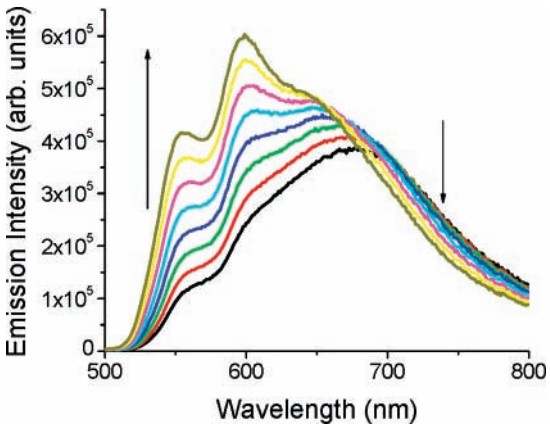

Figure 5. Fluorescence spectra of **2b** in toluene, excitation at 490 nm. Spectra at 10 °C intervals. −10 °C (black), 0 °C (red), 10 °C (green), 20 °C (blue), 30 °C (cyan), 40 °C (magenta), 50 °C (yellow), and 60 °C (dark yellow).

The steady-state emission spectra of **4**, **5a**, **5b**, and **6** in toluene are provided in Figure 6. The emission maximum of **4** occurs at 568 nm with vibronic bands at 611 and 675 nm. The emission spectrum of **5a** is broad, featureless, and highly red-shifted relative to that of the monomer, with an emission maximum occurring at 705 nm. The emission spectrum of **5b** at 675 nm is blue-shifted relative to that of **5a**, while the emission band for **6** has a 679 nm maximum.

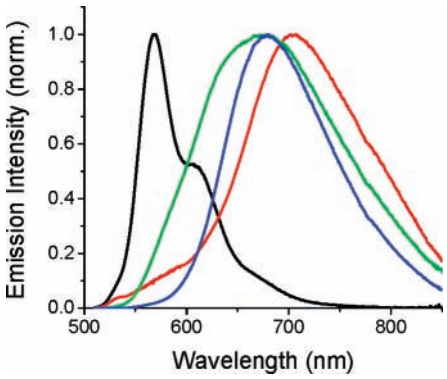

Figure 6. Fluorescence spectra of **4** (black), **5a** (red), **5b** (green), and **6** (blue) in toluene, excitation at 500 nm.

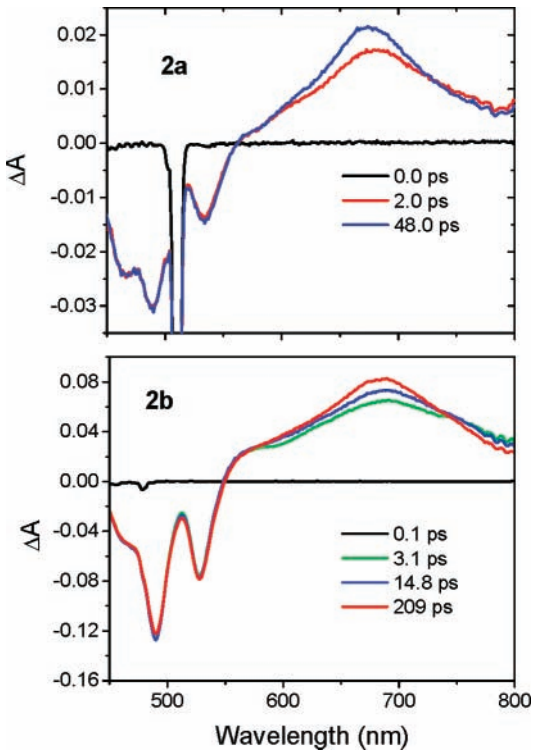

Figure 7. Femtosecond transient absorption spectra in toluene following excitation at 475 nm for **2a** and 510 nm for **2b**. The sharp negative ΔA features at 475 nm in the spectra of **2a** are scattered excitation light.

Time-Resolved Absorption and Emission Spectroscopy. Femtosecond transient absorption spectra of **2a** and **2b** in toluene following 510 nm, 120 fs excitation are shown in Figure 7. Photoexcitation of **2a** and **2b** results in a ground-state bleach from 450 to 550 nm, which is accompanied by broad transient absorption features that extend from 550 to 800 nm. For **2a**, this absorption exhibits a broad maximum at 681 nm immediately after excitation, which blue-shifts to 676 nm with $\tau = 1.2 \pm 0.2$ ps, while for **2b**, a similar spectral evolution takes place with the initial maximum at 691 nm shifting to 686 nm with $\tau = 69 \pm 10$ ps. The resulting transient absorption spectra for both **2a** and **2b** are longer-lived than the 6 ns maximum pump−probe delay time available using the femtosecond transient absorption apparatus, so that nanosecond transient absorption measurements were used to show that the 676 nm band of **2a** decays within the 7 ns instrument response, while the 686 nm band of **2b** decays with $\tau = 29 \pm 1$ ns (not shown). The femtosecond transient absorption spectrum of trimer **3** has a ground-state bleach that extends from 420 to 560 nm, but is

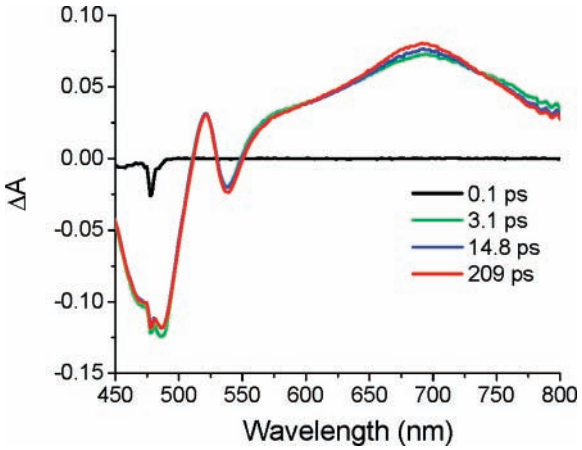

Figure 8. Transient absorption spectra of **3** in toluene following excitation at 475 nm.

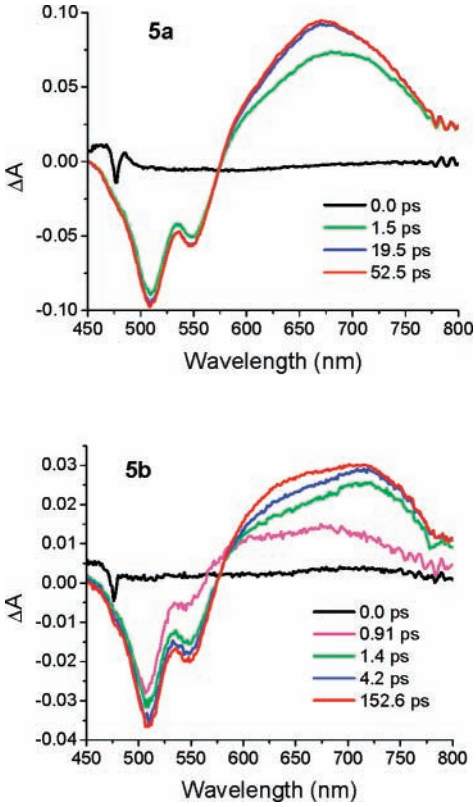

Figure 9. Transient absorption spectra of **5a** and **5b** in toluene following excitation at 475 nm.

interrupted by an absorption feature at 530 nm, Figure 8. The initial absorption exhibits a broad maximum at 698 nm immediately after excitation, which blue-shifts to 694 nm with $\tau = 50 \pm 12$ ps, followed by a $\tau = 25 \pm 2$ ns decay. Femtosecond transient absorption spectra of **5a** and **5b** in toluene are characterized by ground-state bleaching from 450 to 575 nm, Figure 9. Photoexcitation of **5a** results in immediate formation of a spectrum with a broad maximum at 689 nm, which blue-shifts with $\tau = 5.0 \pm 0.5$ ps to 675 nm, then decays with $\tau = 22 \pm 1$ ns. In contrast, photoexcitation of **5b** results in immediate formation of a spectrum with a broad maximum at 678 nm, which red-shifts with $\tau = 5 \pm 0.5$ ps to 715 nm, then decays with $\tau = 18 \pm 1$ ns for **5b**. The transient absorption spectra of **6** in toluene following 475 nm excitation, Figure 10, are characterized by ground-state bleaching at 510 nm accompanied by a broad absorption feature at 580−800 nm. The

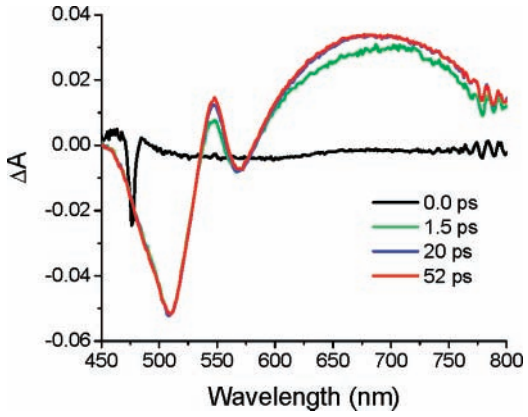

Figure 10. Transient absorption spectra of **6** in toluene following excitation at 475 nm.

bleach extends to 570 nm and is interrupted by a positive absorbance feature that appears at 546 nm. The initial positive absorption changes exhibit a broad 700 nm maximum, which blue-shifts to 687 nm with $\tau = 2 \pm 0.2$ ps, then decays with $\tau = 39 \pm 1$ ns.

The emission decay lifetimes of the PDI and PPDI monomers, dimers, and trimers in toluene at room temperature excited with 400 nm laser pulses are presented in Table 1. The fluorescence lifetimes of monomers **1** and **4** are 3.8 and 4.5 ± 0.1 ns, respectively, and are typical of monomeric PDI derivatives.[72] A wavelength-independent, monoexponential emission lifetime of $\tau = 9.2 \pm 0.1$ ns was observed for dimer **2a**, while that from **2b** was wavelength-dependent with $\tau = 50 \pm 10$ ps at 550 nm and $\tau = 28.6 \pm 0.1$ ns at 700 nm. The wavelength-dependent emission decay times for trimer **3** are similar to those of dimer **2b**, while for **5a**, **5b**, and **6** the emission decay times are all long and essentially wavelength-independent, Table 1.

Discussion

PDI and PPDI Dimers. The optical properties of molecules containing multiple identical chromophores are strongly dependent on the relative orientation and distance between the adjacent chromophores. The zero-order molecular exciton model[73] predicts that coupling of the transition dipole moments creates two new exciton states. For cofacially stacked chromophores having parallel transition moments (so-called *H*-aggregates), the transition from the ground state to the higher energy exciton state is fully allowed, while the transition to the lower exciton state is forbidden. The transition dipoles of the PDI and PPDI chromophores in the dimers and trimers studied in this work are constrained to conformations close to a cofacial, parallel orientation by the rigid structure of the xanthene scaffold. Because the transition dipoles for PDI and PPDI lie along their N−N axes,[71] the exciton model explains the enhanced blue-shifted bands observed for the dimers and trimers. Extension of this model to include vibronic coupling modifies the selection rules for the zero-order exciton states.[74−79] For example, the 491 nm band of **2b** is assigned as the transition from the $\nu = 0$ ground-state vibronic level to the $\nu = 0$ vibronic level of the upper exciton state, while the 530 nm band is assigned to the transition from the $\nu = 0$ ground-state vibronic level to the $\nu = 1$ vibronic band of the lower exciton state.

While a similar assignment can be made for the other dimer and trimer molecules, there are differences in the energies, bandwidths, and relative intensities of their absorption spectra that can be attributed to structural differences among the

molecules. For example, the $\nu = 1$ lower exciton state absorbance peaks are at 531 and 527 nm for PDI dimers **2a** and **2b**, respectively. The peak for **2b** is more intense and narrower than that of **2a**, while the energy separation between the two lowest absorption peaks is slightly greater in **2a** as compared to that in **2b**. These observations suggest that the exciton coupling between adjacent chromophores in ^{1}***2a** is slightly stronger than that in ^{1}***2b**. It is likely that the transition moments for the PDI chromophores within ^{1}***2a** are more closely parallel to each other than are those in ^{1}***2b**, wherein steric interactions between the 12-tricosanyl groups may interfere somewhat with the optimal geometry for exciton coupling. The UV−vis spectra of PPDI dimers **5a** and **5b** have similar vibronic peak spacings and intensity ratios, indicating that structural differences between them that affect their exciton interaction are also modest.

Broad, featureless, red-shifted emission spectra have been observed previously in tethered PDI oligomers,[41,46] cyclophanes,[35] and self-assembled systems.[65] The observed emission for **2a** is assigned to an excimer-like state. In a classical excimer, the molecules are only associated after one of the chromophores is excited and subsequently forms a complex with a chromophore in the ground state. The emission maximum of **2a** is red-shifted ~5300 cm^{-1} relative to the monomer fluorescence maximum, comparable to the largest shifts observed for excimers of aromatic compounds that are tethered together by flexible alkyl chains.[80−82] For those compounds, the optimal geometry is achieved by π-stacking with only partial overlap of the π-systems of the aromatic compounds.

The emission spectrum of **2b** is unusual in that it contains both a red-shifted featureless component as well as two resolved shoulders on the blue edge of the band. The shoulders at 561 and 611 nm in the **2b** emission spectrum do not correspond to the emission peaks observed in the emission spectrum of monomer **1** and are narrow as compared to those of typical excimers. Moreover, these bands mirror the vibronic structure of the absorption band of **2b**, so that these emission bands most likely originate from the lower exciton state. As noted above, the exciton coupling model predicts that emission from the lower energy state is symmetry forbidden when the transition dipoles are parallel. The bulky 12-tricosanyl groups on **2b** likely force the PDI chromophores into an excited-state geometry in which the chromophores are both farther apart than in **2a** and in which their transition dipoles are no longer parallel. These structural changes result in an orientation of the two chromophores in which the transition from the lower exciton state to the ground state becomes partially allowed.[73,79,83]

The fluorescence spectra of **2a** and **2b** show that the energy of the excimer-like state is lower than that of the lower exciton state. This suggests that it may be possible to observe the kinetics of formation of the excimer-like state from the lower exciton state. The excimer-like emission from **2a** decays with $\tau = 9.2 \pm 0.1$ ns, which is constant across the emission band, while the lower exciton state fluorescence from **2b** decays with $\tau = 50 \pm 10$ ps at 550 nm and the excimer-like state emits with a decay time of $\tau = 28.6 \pm 0.1$ ns at 700 nm. The transient absorption spectra given in Figure 7 show that the initial absorption peak of **2a** shifts from 681 to 676 nm with $\tau = 1.2 \pm 0.2$ ps, while that of **2b** shifts from 691 nm to 686 and broadens with $\tau = 69 \pm 10$ ps. The 1.2 ps process in **2a** may be due to formation of the excimer-like state from the lower exciton state. However, we did not observe the corresponding rapid emission decay due to the 20 ps time resolution of our apparatus. On the other hand, the 69 ps formation time constant for the 686 nm band in **2b** agrees within experimental error with the measured emission lifetime of its lower exciton state. Moreover, the 686 nm band is significantly broadened relative to those of the corresponding excited-state absorption bands for PDI monomers, which is characteristic of π-stacked *H*-aggregates of PDI chromophores.[72] The lifetime of the excimer-like state in **2a** is shorter than that of **2b** due largely to increased nonradiative decay in **2a** because the sterically less-demanding *n*-octyl groups permit stronger electronic interaction between the two PDI molecules.

To better understand the emissive pathways in **2b**, the temperature dependence of its steady-state emission spectrum was determined, Figure 5. The spectra reveal that the excimer-like emission, which is assigned to the longer wavelength component of the emission band, dominates at low temperatures, while fluorescence from the lower exciton state is the major emissive pathway at higher temperatures. In addition, the excimer-like emission red-shifts as the temperature is lowered. This trend is physically reasonable given that at higher temperatures, an increase in the conformational mobility of the PDI chromophores on the xanthene bridge would result in a decrease in population of molecules that achieve the optimal geometry for excimer formation under the constraints imposed by the xanthene spacer, thus leading to competitive emission from the lower exciton state.

Another way to modify the degree to which two PDI molecules can π-stack is to add groups to their bay region positions. In **5a** and **5b**, 3,5-di-*t*-butylphenoxy groups are positioned at the 1,7-positions of PDI, while sterically less-demanding *n*-octyl groups (based on the behavior of **2a**) are attached to the imide nitrogen atoms. The staggered conformation of the phenoxy groups in **5a** permits the π systems of the two chromophores to interact more strongly, resulting in an excimer-like state with a lower energy emission relative to that of **5b**. In addition, the fluorescence spectrum of **5a** shows a weak band at 585 nm that may be due to emission from its lower exciton state. On the other hand, the spectrum of **5b** has significant shoulders on its blue edge, which indicate that the quantum yield of emission from its lower exciton state relative to that of its excimer-like state is somewhat higher than that of **5a**. This is consistent with the idea that the steric interactions of the eclipsing phenoxy groups in **5b** distort its excited-state structure further away from the parallel cofacial geometry than do the staggered phenoxy groups in **5a**, resulting in a somewhat increased transition probability for emission from the lower exciton state in **5b** relative to that in **5a**. The fluorescence lifetime measurements did not clearly resolve the short emission components that are expected to result from decay of the lower exciton states of **5a** and **5b** to their respective excimer-like states at the bluer wavelengths of the emission band.

The transient absorption spectra of **5a** and **5b**, Figure 9, show broad features in the 600−800 nm wavelength range similar to those of **2a** and **2b**. The transient absorption spectrum of **5a** appears initially at 684 nm and blue-shifts to 675 nm with $\tau = 5.0 \pm 0.5$ ps, while the initial spectrum of **5b** appears at 715 nm and broadens mostly by filling in the spectral region from 620 to 670 nm with $\tau = 5.0 \pm 0.5$ ps. These short transients are most likely due to structural relaxations within **5a** and **5b** required to form their excimer-like states, but could contain contributions from vibrational relaxation as well. Fluorescence emission from the excimer-like states of **5a** and **5b** exhibits monoexponential decays with lifetimes of $\tau = 21 \pm 1$ ns and $\tau = 19 \pm 1$ ns, respectively. The lifetimes of these states are corroborated by nanosecond transient absorption data, which

yield decay times within experimental error of those observed by emission decay (see Results). These lifetimes are more than twice as long as the lifetime of **2a** and are somewhat shorter than that of **2b**. The lifetimes of **5a** and **5b** suggest that the strengths of the electronic interactions between the two PPDI molecules in their excimer-like states are intermediate to those of **2a** and **2b**. This is most likely due to the increased steric hindrance provided by the phenoxy groups, which prevent the tight association present in **2a**, while allowing a more favorable interaction than do the 12-tricosanyl substituents on the imide nitrogen atoms in **2b**.

We have calculated the energy-minimized ground-state structures of **2a**, **2b**, **5a**, and **5b** using the semiempirical PM3 molecular orbital method[84] to determine whether the observed differences in their excited-state behavior originate from ground-state structural differences between them or must be attributed to excited-state geometries that differ from those of the ground state, Figure S4. The average calculated interplanar distances between the PDI molecules in **2a** and **2b** are 4.4 and 4.5 Å, respectively, while those of **5a** and **5b** are both 4.8 Å. The C−C distances between all pairs of sp^2 carbon atoms in which one atom is on each PDI of the dimer are all >4.3 Å. The torsional angles between the N−N axes of the PDI chromophores in **2a** and **2b** are 5.1° and 6.9°, respectively, while those of the PPDI chromophores in **5a** and **5b** are 2.3° and 8.9°, respectively. These calculations suggest that the ground-state structures of **2a** and **2b** are very similar despite the presence of the more sterically demanding branched alkyl group on the PDI nitrogen atoms of **2b**. The average calculated interplanar spacings of the PPDI chromophores in **5a** and **5b** are the same and are only slightly larger than those calculated for **2a** and **2b**. The only significant calculated structural difference between **5a** and **5b** is the somewhat larger torsional angle in **5b** required to accommodate the eclipsed conformation of the 1,7-phenoxy substituents of the PPDI chromophores. Once again, these ground-state differences are rather small, so that the observed excited-state properties presumably reflect more significant changes in the excited-state structures.

PDI and PPDI Trimers. Trimer **3** is structurally similar to **2b** in that the imides of the outer PDI molecules are terminated in 12-tricosanyl groups. Unlike **2b**, however, the *t*-butyl groups on the xanthene provide enhanced steric interactions with the bulky 12-tricosanyl groups. Nevertheless, the UV−vis spectrum of **3** exhibits a slightly larger energy splitting between the first and second vibronic bands. This observation suggests that the exciton coupling between the three PDI chromophores in the trimer is only modestly increased over that in dimers **2a** and **2b**. The fluorescence quantum yield of trimer **3** is about 70% that of **2b**; it exhibits a 50 ps decay at 550 nm similar to that of **2b**, and its excimer-like state has a 22.5 ns decay at 700 nm, which is about 77% as long as that of **2b**. The fluorescence data for **3** are once again corroborated by the transient absorption measurements, where an initial slight blue-shift of the transient spectrum takes place with $\tau = 50 \pm 12$ ps followed by a long $\tau = 25 \pm 2$ ns decay of the excimer-like state. Thus, the small decrease in quantum yield for **3** relative to that of **2b** is due mostly to the lower fluorescence quantum yield of its excimer-like state. While Li and co-workers have also observed a decrease in the fluorescence quantum yields of larger π-stacked PDI oligomers,[85] the similar photophysical behavior of dimer **2b** and trimer **3** suggests that the formation and decay of the excimer-like state within **3** most likely involves a strong interaction between only two of its PDI molecules. The involvement of principally two PDI molecules in the excimer-like state does not contradict the observed larger exciton interaction in trimer **3** versus dimer **2b** because the exciton interaction is a dipole−dipole interaction, whereas the formation of the excimer-like state depends on orbital overlap between the PDI molecules.

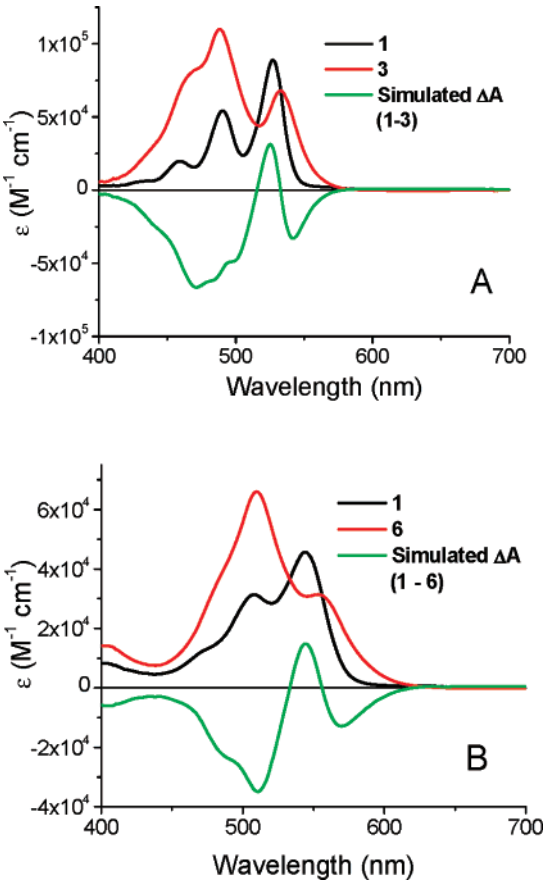

Figure 11. Simulated transient absorption spectra in toluene of (A) trimer **3** and (B) trimer **6**.

In trimer **6**, the inner and one of the outer PPDI molecules have their phenoxy groups in an eclipsed conformation, while the inner PPDI and the other outer PPDI have their phenoxy groups in the staggered conformation. Steric repulsion between the imide alkyl groups and the xanthene is minimized by using *n*-octyl groups on the imides and removing the *t*-butyl groups from the xanthenes, which potentially allows for better cofacial $\pi-\pi$ stacking of the PPDI chromophores. The excimer-like emission from **6** has a fluorescence quantum yield that is about 3−4 times greater than those of **5a** and **5b**, while the fluorescence lifetime of **6** is only about 2 times longer than those of **5a** and **5b**, Table 1. The transient absorption spectra of **6** are characterized by immediate formation of a broad absorption feature with a maximum at 700 nm, which blue-shifts to 687 nm with $\tau = 2 \pm 0.2$ ps, then decays with $\tau = 37 \pm 1$ ns. Once again, the transient absorption data corroborate fluorescence lifetime of the excimer-like state of **6**. The small blue-shift in the transient absorption spectra on the picosecond time scale may again be due to structural relaxations, which permit rapid access to the excimer-like state following photoexcitation, as well as contributions from vibrational relaxation. The disproportionate increases in the fluorescence quantum yield and lifetime of the excimer-like state of **6** suggest that its geometry differs from that of **5a** and **5b** in a way that changes both its radiative and its nonradiative (and/or intersystem crossing) decay rates. This may be a consequence of increased chromophore rigidity enforced by the trimer structure.

The apparent involvement of only two chromophores within the excimer-like state of trimers **3** and **6** implies that one chromophore is not strongly coupled to the other two. To test this hypothesis, the transient absorption spectra of **3** and **6** were simulated by subtracting their ground-state absorption spectra from the ground-state absorption spectra of monomers, **1** and **4**, respectively. The simulated transient absorption spectra of **3** and **6** are shown in Figure 11. These simulations predict positive transient absorption features at 525 nm for **3** and 544 nm for **6**, which are very close to the observed positive features measured for **3** and **6** at 530 and 546 nm, respectively, Figures 9 and 10. These simulations deviate from the transient absorption spectra at longer wavelengths because the excited-state absorptions are not included in them. The positive transient absorption features are only found in the trimers as opposed to the dimers and suggest that the formation of the observed excimer-like states in **3** and **6** results largely from chromophore dimer interactions within these trimers and that the addition of a third chromophore does not ensure that the entire trimer ensemble has structural features that optimize longer-range electronic interactions.[86]

Conclusions

We have characterized the photophysics of a series of cofacially oriented, *H*-stacked PDI and PPDI dimer and trimers. In the PDI series, the groups at the imide position are important for determining the excited-state energetics and dynamics of these molecules. Placing *n*-octyl groups on the imide nitrogen atoms of the PDI chromophores results in near optimal π-stacking, leading to formation of a low-energy excimer-like state, while substituting the more sterically demanding 12-tricosanyl group on the imides causes deviations from the optimum that results in slower formation of an excimer-like excited state having somewhat higher energy. By comparison, the two isomeric PPDI dimers having terminal *n*-octyl imide groups have photophysical properties that depend on the ability of the phenoxy groups to modify the π stacking of the PPDI molecules. In general, disruption of optimal π-stacking by steric interactions of the phenoxy side groups results in excimer-like states that are higher in energy. The corresponding lowest excited singlet states of PDI and PPDI trimers are dimer-like in nature and suggest that the structural distortions that accompany formation of the trimers are sufficient to confine the electronic interaction on two chromophores within these systems. This further suggests that it may be useful to build into oligomeric PDI and PPDI systems some degree of flexibility that allows the structural relaxations necessary to optimize the electronic interactions between multiple chromophores.

Acknowledgment. This research was supported by the Chemical Sciences, Geosciences, and Biosciences Division, Office of Basic Energy Sciences, DOE under grant no. DE-FG02-99ER14999. J.V.L. acknowledges the donors of the American Chemical Society Petroleum Research Fund for partial support of this research. We thank Dr. D. W. McCamant for carrying out preliminary experiments.

Supporting Information Available: Experimental details, including the synthesis and characterization of the molecules, modeling, and transient absorption. This material is available free of charge via the Internet at http://pubs.acs.org.

References and Notes

(1) Brown, A. R.; Jarrett, C. P.; deLeeuw, D. M.; Matters, M. *Synth. Met.* **1997**, *88*, 37−55.
(2) Dimitrakopoulos, C. D.; Purushothaman, S.; Kymissis, J.; Callegari, A.; Shaw, J. M. *Science* **1999**, *283*, 822−824.
(3) Katz, H. E. *J. Mater. Chem.* **1997**, *7*, 369−376.
(4) Würthner, F. *Angew. Chem., Int. Ed.* **2001**, *40*, 1037−1039.
(5) Anthony, J. E.; Eaton, D. L.; Parkin, S. R. *Org. Lett.* **2002**, *4*, 15−18.
(6) Horowitz, G. *Adv. Mater.* **1998**, *10*, 365−377.
(7) Payne, M. M.; Delcamp, J. H.; Parkin, S. R.; Anthony, J. E. *Org. Lett.* **2004**, *6*, 1609−1612.
(8) Gregg, B. A.; Fox, M. A.; Bard, A. J. *J. Phys. Chem.* **1990**, *94*, 1586−1597.
(9) Hasobe, T.; Imahori, H.; Kamat, P. V.; Ahn, T. K.; Kim, S. K.; Kim, D.; Fujimoto, A.; Hirakawa, T.; Fukuzumi, S. *J. Am. Chem. Soc.* **2005**, *127*, 1216−1228.
(10) Tang, C. W. *Appl. Phys. Lett.* **1986**, *48*, 183−185.
(11) Cogdell, R. J.; Isaacs, N. W.; Freer, A. A.; Howard, T. D.; Gardiner, A. T.; Prince, S. M.; Papiz, M. Z. *FEBS Lett.* **2003**, *555*, 35−39.
(12) Herman, P.; Kleinekathofer, U.; Barvik, I.; Schreiber, M. *J. Lumin.* **2001**, *94*, 447−450.
(13) Dahlbom, M.; Pullerits, T.; Mukamel, S.; Sandstrom, V. *J. Phys. Chem. B* **2001**, *105*, 5515−5524.
(14) Lewis, F. D.; Kalgutkar, R. S.; Wu, Y.; Liu, X.; Liu, J.; Hayes, R. T.; Miller, S. E.; Wasielewski, M. R. *J. Am. Chem. Soc.* **2000**, *122*, 12346−12351.
(15) Lewis, F. D.; Liu, J.; Weigel, W.; Rettig, W.; Kurnikov, I. V.; Beratan, D. N. *Proc. Natl. Acad. Sci. U.S.A.* **2002**, *99*, 12536−12541.
(16) Lewis, F. D.; Wu, T.; Zhang, Y.; Letsinger, R. L.; Greenfield, S. R.; Wasielewski, M. R. *Science* **1997**, *277*, 673−676.
(17) Prathapan, S.; Yang, S. I.; Seth, J.; Miller, M. A.; Bocian, D. F.; Holten, D.; Lindsey, J. S. *J. Phys. Chem. B* **2001**, *105*, 8237−8248.
(18) Yang, S. I.; Prathapan, S.; Miller, M. A.; Seth, J.; Bocian, D. F.; Lindsey, J. S.; Holten, D. *J. Phys. Chem. B* **2001**, *105*, 8249−8258.
(19) Tomizaki, K.; Loewe, R. S.; Kirmaier, C.; Schwartz, J. K.; Retsek, J. L.; Bocian, D. F.; Holten, D.; Lindsey, J. S. *J. Org. Chem.* **2002**, *67*, 6519−6534.
(20) Muthukumaran, K.; Loewe, R. S.; Kirmaier, C.; Hindin, E.; Schwartz, J. K.; Sazanovich, I. V.; Diers, J. R.; Bocian, D. F.; Holten, D.; Lindsey, J. S. *J. Phys. Chem. B* **2003**, *107*, 3431−3442.
(21) Miller, M. A.; Lammi, R. K.; Prathapan, S.; Holten, D.; Lindsey, J. S. *J. Org. Chem.* **2000**, *65*, 6634−6649.
(22) Chen, S.-G.; Stradins, P.; Gregg, B. A. *J. Phys. Chem. B* **2005**, *109*, 13451−13460.
(23) Chen, S. G.; Branz, H. M.; Eaton, S. S.; Taylor, P. C.; Cormier, R. A.; Gregg, B. A. *J. Phys. Chem. B* **2004**, *108*, 17329−17336.
(24) Gregg, B. A. *J. Phys. Chem. B* **2003**, *107*, 4688−4698.
(25) Neuteboom, E. E.; Meskers, S. C. J.; Van Hal, P. A.; Van Duren, J. K. J.; Meijer, E. W.; Janssen, R. A. J.; Dupin, H.; Pourtois, G.; Cornil, J.; Lazzaroni, R.; Bredas, J.-L.; Beljonne, D. *J. Am. Chem. Soc.* **2003**, *125*, 8625−8638.
(26) Gregg, B. A.; Cormier, R. A. *J. Am. Chem. Soc.* **2001**, *123*, 7959−7960.
(27) Dittmer, J. J.; Marseglia, E. A.; Friend, R. H. *Adv. Mater.* **2000**, *12*, 1270−1274.
(28) Ferrere, S.; Zaban, A.; Gregg, B. A. *J. Phys. Chem. B* **1997**, *101*, 4490−4493.
(29) Ford, W. E.; Kamat, P. V. *J. Phys. Chem.* **1987**, *91*, 6373−6380.
(30) Ford, W. E.; Hiratsuka, H.; Kamat, P. V. *J. Phys. Chem.* **1989**, *93*, 6692−6696.
(31) Würthner, F.; Thalacker, C.; Sautter, A. *Adv. Mater.* **1999**, *11*, 754−758.
(32) Langhals, H.; Saulich, S. *Chem.-Eur. J.* **2002**, *8*, 5630−5643.
(33) Schenning, A. P. H. J.; van Herrikhuyzen, J.; Jonkheijm, P.; Chen, Z.; Würthner, F.; Meijer, E. W. *J. Am. Chem. Soc.* **2002**, *124*, 10252−10253.
(34) Kirmaier, C.; Hindin, E.; Schwartz, J. K.; Sazanovich, I. V.; Diers, J. R.; Muthukumaran, K.; Taniguchi, M.; Bocian, D. F.; Lindsey, J. S.; Holten, D. *J. Phys. Chem. B* **2003**, *107*, 3443−3454.
(35) Langhals, H.; Ismael, R. *Eur. J. Org. Chem.* **1998**, 1915−1917.
(36) Ahrens, M. J.; Fuller, M. J.; Wasielewski, M. R. *Chem. Mater.* **2003**, *15*, 2684−2686.
(37) Zhao, Y.; Wasielewski, M. R. *Tetrahedron Lett.* **1999**, *40*, 7047−7050.
(38) Ahrens, M. J.; Sinks, L. E.; Rybtchinski, B.; Liu, W.; Jones, B. A.; Giaimo, J. M.; Gusev, A. V.; Goshe, A. J.; Tiede, D. M.; Wasielewski, M. R. *J. Am. Chem. Soc.* **2004**, *126*, 8284−8294.
(39) Thalacker, C.; Würthner, F. *Adv. Funct. Mater.* **2002**, *12*, 209−218.
(40) van der Boom, T.; Hayes, R. T.; Zhao, Y.; Bushard, P. J.; Weiss, E. A.; Wasielewski, M. R. *J. Am. Chem. Soc.* **2002**, *124*, 9582−9590.
(41) Wang, W.; Li, L. S.; Helms, G.; Zhou, H. H.; Li, A. D. Q. *J. Am. Chem. Soc.* **2003**, *125*, 1120−1121.
(42) Wang, W.; Han, J. J.; Wang, L. Q.; Li, L. S.; Shaw, W. J.; Li, A. D. Q. *Nano Lett.* **2003**, *3*, 455−458.

(43) Würthner, F. *Chem. Commun.* **2004**, 1564−1579.
(44) Yan, P.; Chowdhury, A.; Holman, M. W.; Adams, D. M. *J. Phys. Chem. B* **2005**, *109*, 724−730.
(45) Han, J. J.; Wang, W.; Li, A. D. Q. *J. Am. Chem. Soc.* **2006**, *128*, 672−673.
(46) Neuteboom, E. E.; Meskers, S. C. J.; Meijer, E. W.; Janssen, R. A. J. *Macromol. Chem. Phys.* **2004**, *205*, 217−222.
(47) Datar, A.; Oitker, R.; Zang, L. *Chem. Commun.* **2006**, 1649−1651.
(48) Dehm, V.; Chen, Z.; Baumeister, U.; Prins, P.; Siebbeles, L. D. A.; Würthner, F. *Org. Lett.* **2007**, *9*, 1085−1088.
(49) Zhan, X.; Tan, Z. a.; Domercq, B.; An, Z.; Zhang, X.; Barlow, S.; Li, Y.; Zhu, D.; Kippelen, B.; Marder, S. R. *J. Am. Chem. Soc.* **2007**, *129*, 7246−7247.
(50) Che, Y.; Datar, A.; Balakrishnan, K.; Zang, L. *J. Am. Chem. Soc.* **2007**, *129*, 7234−7235.
(51) Che, Y.; Datar, A.; Yang, X.; Naddo, T.; Zhao, J.; Zang, L. *J. Am. Chem. Soc.* **2007**, *129*, 6354−6355.
(52) Yagai, S.; Monma, Y.; Kawauchi, N.; Karatsu, T.; Kitamura, A. *Org. Lett.* **2007**, *9*, 1137−1140.
(53) Würthner, F.; Hanke, B.; Lysetska, M.; Lambright, G.; Harms, G. S. *Org. Lett.* **2005**, *7*, 967−970.
(54) Würthner, F.; Sautter, A. *J. Chem. Soc., Chem. Commun.* **2000**, 445−446.
(55) Kaiser, T. E.; Wang, H.; Stepanenko, V.; Würthner, F. *Angew. Chem., Int. Ed.* **2007**, *46*, 5541−5544, S5541/5541−S5541/5513.
(56) Chen, Z.; Baumeister, U.; Tschierske, C.; Würthner, F. *Chem.-Eur. J.* **2007**, *13*, 450−465.
(57) Li, X.; Sinks, L. E.; Rybtchinski, B.; Wasielewski, M. R. *J. Am. Chem. Soc.* **2004**, *126*, 10810−10811.
(58) Zhang, J.; Hoeben, F. J. M.; Pouderoijen, M. J.; Schenning, A. P. H.; Meijer, E. W.; Schryver, F. C.; De Feyter, S. *Chem.-Eur. J.* **2006**, *12*, 9046−9055.
(59) Rybtchinski, B.; Sinks, L. E.; Wasielewski, M. R. *J. Phys. Chem. A* **2004**, *108*, 7497−7505.
(60) Rybtchinski, B.; Sinks, L. E.; Wasielewski, M. R. *J. Am. Chem. Soc.* **2004**, *126*, 12268−12269.
(61) Wasielewski, M. R. *J. Org. Chem.* **2006**, *71*, 5051−5066.
(62) Li, X.; Sinks, L. E.; Rybtchinski, B.; Wasielewski, M. R. *J. Am. Chem. Soc.* **2004**, *126*, 10810−10811.
(63) van der Boom, T.; Hayes, R. T.; Zhao, Y.; Bushard, P. J.; Weiss, E. A.; Wasielewski, M. R. *J. Am. Chem. Soc.* **2002**, *124*, 9582−9590.
(64) Hamann, B. C.; Branda, N. R.; Rebek, J., J. *Tetrahedron Lett.* **1993**, *34*, 6837−6840.
(65) Hernando, J.; de Witte, P. A. J.; van Dijk, E. M. H. P.; Korterik, J.; Nolte, R. J. M.; Rowan, A. E.; Garcia-Parajo, M. F.; van Hulst, N. F. *Angew. Chem., Int. Ed.* **2004**, *43*, 4045−4049.
(66) Ahrens, M. J.; Kelley, R. F.; Dance, Z. E. X.; Wasielewski, M. R. *Phys. Chem. Chem. Phys.* **2007**, *9*, 1469−1478.
(67) Sens, R.; Drexhage, K. H. *J. Lumin.* **1981**, *24*−*5*, 709−712.
(68) Kubin, R. F.; Fletcher, A. N. *J. Lumin.* **1982**, *27*, 455−462.
(69) Giaimo, J. M.; Gusev, A. V.; Wasielewski, M. R. *J. Am. Chem. Soc.* **2002**, *124*, 8530−8531.
(70) Pshenichnikov, M. S.; de Boerij, W. P.; Wiersma, D. A. *Opt. Lett.* **1994**, *19*, 572−575.
(71) Hennessy, M. H.; Soos, Z. G.; Pascal, R. A.; Girlando, A. *Chem. Phys.* **1999**, *245*, 199−212.
(72) Ahrens, M. J.; Sinks, L. E.; Rybtchinski, B.; Liu, W.; Jones, B. A.; Giaimo, J. M.; Gusev, A. V.; Goshe, A. J.; Tiede, D. M.; Wasielewski, M. R. *J. Am. Chem. Soc.* **2004**, *126*, 8284−8294.
(73) Kasha, M.; Rawles, H. R.; El-Bayoumi, M. L. *Pure Appl. Chem.* **1965**, *11*, 371−392.
(74) Fulton, R. L.; Gouterman, M. *J. Chem. Phys.* **1964**, *41*, 2280−2286.
(75) Oddos-Marcel, L.; Madeore, F.; Bock, A.; Neher, D.; Ferencz, A.; Rengel, H.; Wegner, G.; Kryschi, C.; Trommsdorff, H. P. *J. Phys. Chem.* **1996**, *100*, 11850−11856.
(76) Myers-Kelley, A. *J. Chem. Phys.* **2003**, *119*, 3320−3331.
(77) Seibt, J.; Marquetand, P.; Engel, V.; Chen, Z.; Dehm, V.; Würthner, F. *Chem. Phys.* **2006**, *328*, 354−362.
(78) Seibt, J.; Dehm, V.; Wurthner, F.; Engel, V. *J. Chem. Phys.* **2007**, *126*, 164308/164301−164308/164306.
(79) Clark, A. E.; Qin, C.; Li, A. D. Q. *J. Am. Chem. Soc.* **2007**, *129*, 7586−7595.
(80) Birks, J. B.; Munro, I. H.; Lumb, M. D. *Proc. R. Soc. London, Ser. A* **1964**, *280*, 289.
(81) Hayashi, T.; Mataga, N.; Umemoto, T.; Sakata, Y.; Misumi, S. *J. Phys. Chem.* **1977**, *81*, 424−429.
(82) Ohkita, H.; Ito, S.; Yamamoto, M.; Tohda, Y.; Tani, K. *J. Phys. Chem. A* **2002**, *106*, 2140−2145.
(83) Manas, E. S.; Spano, F. C. *J. Chem. Phys.* **1998**, *109*, 8087−8101.
(84) *Hyperchem*; Hypercube Inc., 1115 NW 4th St., G., FL 32601.
(85) Li, A. D. Q.; Wang, W.; Wang, L.-Q. *Chem.-Eur. J.* **2003**, *9*, 4594−4601.
(86) Nakano, T.; Yade, T. *J. Am. Chem. Soc.* **2003**, *125*, 15474−15484.